Coarsening and Dissolution of γ′ precipitates during Solution Treatment of AD730™ Ni-based Superalloy: Mechanisms and Kinetics Models

F. Masoumi[a,*], M. Jahazi[a], D. Shahriari[a], J. Cormier[b]

[a] Department of Mechanical Engineering, École de Technologie Supérieure (ETS), H3C 1K3, Montreal, QC, Canada

[b] Institute Pprime, UPR CNRS 3346, Physics and Mechanics of Materials Department, ISAE- ENSMA, BP 40109, Futuroscope- Chasseneuil Cedex 86961, France

[*] Fatemeh.Masoumi.1@ens.etsmtl.ca

Abstract

The kinetics of γ′ size and volume fraction changes during solution treatment of the advanced Ni-based superalloy, AD730™ are determined and the underlying mechanisms are investigated. High resolution Differential Thermal Analysis (DTA) and thermodynamic modeling were used to design and perform solution heat treatment experiments. Semi-analytical models are developed to describe the dissolution and coarsening processes. The results from the proposed models, supported by electron microscopy observations, indicate that coarsening occurs before complete dissolution takes place. Agglomeration is shown to be the governing coarsening mechanism for this alloy after calculation of the coefficients for both the Ostwald ripening and agglomeration mechanisms. Electron microscopy observations revealed that the early stages of agglomeration occur by neck formation between two neighboring particles. The splitting of γ′ particles was identified as one of the main dissolution mechanisms. Based on the obtained results, a dissolution kinetics model is proposed to quantify the volume fraction of dissolved γ′ particles and estimate the activation energy of this process for AD730™. A coarsening model based on the time-temperature dependence of the γ′ coarsening rate coefficient is also proposed taking the concentration of elements, γ′ volume fraction and the temperature into consideration. Based on this model, a method is developed to predict γ′ size evolution during aging heat treatment process and an optimum heat treatment to reach the desired γ′ distribution is proposed. The validity and accuracy of the proposed models were verified by carrying out different heat treatment experiments.

Keywords: Ni-based Superalloys; AD730™; γ′ Phase Dissolution; γ′ Phase Coarsening; Semi-Analytical Modeling; Activation energy

Authors' accepted manuscript of the article published in
Journal of Alloys and Compounds, vol. 658 (2016), p. 981-995
http://dx.doi.org/10.1016/j.jallcom.2015.11.002

1. Introduction

Thermomechanical processes such as rolling, forging, machining and friction welding involve substantial microstructural changes including dissolution and subsequent re-precipitation of γ′ precipitates in Ni-based superalloys. These changes play a key role in controlling the mechanical properties of these alloys. The thermal cycle (heating rate, temperature, and holding time) in addition to accumulated plastic strain and applied stress were found to enhance γ′ dissolution rate in Ni-based superalloys [1-4]. Out of the parameters listed above, the heating stage plays a major role in determining optimum processing parameters. In addition, in thermal processes such as aging and creep, dissolution and coarsening of γ′ have a determining effect in property evolution. Therefore, γ′ size and volume fraction are critical inputs for models of mechanical behavior and microstructure evolution [5-7]. For reliable and accurate kinetics models to be developed, it is necessary to better understand the underlying mechanisms governing γ′ phase evolution during solution heat treatment (SHT).

After solutionizing, aging is carried out to achieve a controlled γ′ phase re-precipitation [8]. Although γ′ reprecipitation during isothermal aging or continuous cooling in Ni-based superalloys has been the subject of extensive research works [9-12], much less attention has been paid to the dissolution kinetics during the heating stage [3, 13]. Hence, the main objective of this research is to accomplish a time and temperature dependent study concerning the evolution of the γ′ phase during the heating stage of the solution heat treatment process.

Theoretically, as suggested by Semiatin et al. [14], the homogenizing should be performed between γ′ solvus and the solidus temperature of the alloy in order to entirely dissolve γ′ and other phases. This approach also removes chemical non-uniformity formed during previous preparation processes. However, solution heat treatments at temperatures high enough to dissolve all the primary γ′ particles have been seriously limited in various superalloys due to the occurrence of incipient melting [15]. To elucidate the influence of the solutionizing temperature on γ′ dissolution kinetics and eliminate possible microstructural damage, both subsolvus and near solvus heat treatments are used in the present investigation.

Thomas et al. [16] presented a theory on the dissolution kinetics of a single precipitate in which dissolution was considered to be approximately the reverse of growth. However, Whelan mentioned that this assumption was not fully accurate [17]. Lifshitz, Slyozov, and Wagner (LSW) [18, 19] proposed an analytical theory describing diffusion-limited coarsening (or

Ostwald ripening) of isolated precipitates. The LSW theory is based on the Gibbs-Thomson equation, which describes that solubility in the small precipitates with a large surface area-to-volume ratio is higher than that for larger precipitates. The larger precipitates, therefore, tend to grow at the expense of the smaller ones to decrease the total interfacial free energy of the alloy. Umantsev, Olson [20] and Philippe et al. [21] expanded the LSW theory to multicomponent systems.

Coarsening and coalescence of γ' precipitates, through application of the LSW theory and particle agglomeration mechanism have been studied in several research works [22, 23]. However, the contributions of these two mechanisms to the dissolution process have not yet been identified nor quantified. Whelan et al. [17] developed an analytical solution for the dissolution of a *single precipitate* under assumptions of stationary interface. This solution can be considered as one of the most accurate analytical solutions to date. However, in real systems, precipitates are often close to each other making it reasonable to assume that some impingement of diffusion fields of neighboring precipitates takes place [24]. This assumption was not taken into account in the Whelan model. In the present study, this aspect is addressed and a model which considers multiple precipitates is presented for dissolution kinetics and validated after a series of experiments.

Wang et al. [13] developed a model to study the influence of initial particle size distribution (PSD) on the dissolution rate of Ni-Al alloys (above the solvus) by using 3D phase field simulations. A critical review of this work indicates that during dissolution the volume fraction of particles decays exponentially with time and while the initial PSD does not affect this trend, the dissolution rate is strongly dependent on PSD. However, computer based simulation methods are generally associated with long computation times and large and expensive infrastructures, particularly when it comes to simulating the behavior of industrial size components. Many physical constants such as element diffusion coefficients, surface energies, interface kinetic coefficients and driving forces for phase transformations are needed for obtaining reliable results. However, this data is not always readily available for alloys with complex compositions [25]. The situation becomes even more complicated when a new alloy, such as the one used in the present investigation, is considered.

Semi-analytical models calibrated by experiments were proposed to address this problem. These models are widely used for characterizing phase precipitation under isothermal and

non-isothermal conditions [26-28] but to the knowledge of the authors, no such models exist for the identification and quantification of the dissolution mechanisms during the solution heat treatment process of Ni-based superalloys. In addition, AD730^{TM} is a newly developed Ni-based superalloy for turbine disk applications with reported superior service properties at 700°C [29-31]. However, many of its properties are unknown for advanced manufacturing applications and especially no quantitative data is available on γ′ dissolution kinetics in AD730^{TM}.

On the basis of the previous analysis, the objectives of this study are three fold:

1- To identify the dissolution temperatures for different populations of γ′ by DTA, Thermo-calc® and heat treatment for AD730^{TM} alloy.

2- To quantify and analyze size distribution and morphology evolution of γ′ precipitates during dissolution process using electron microscopy and image analysis.

3- To propose and validate semi-analytical models for dissolution and coarsening kinetics and calculate the partitioning contribution of various coarsening mechanisms during γ′ dissolution process.

Research results will help to develop a better understanding of fundamental mechanisms governing γ′ dissolution in Ni-based superalloys.

2. Coarsening by agglomeration

Smoluchowski [32] proposed that the agglomeration process can be modeled as an infinite set of second-order reactions. Smaller particles combine to form larger particles, and dissociation is not considered. The rate of change in number density of particle size distribution is given by:

$$\frac{\partial f}{\partial t} = \frac{1}{2}\int_0^v W(v', v-v')f(v',t)f(v-v',t)dv' - f(v,t)\int_0^\infty W(v',v)f(v',t)dv' \qquad (1)$$

where $f(v,t)dv$ is the number density of precipitates per unit volume with particles volumes in the range of $v, v+dv$ and where $W(v',v)$ is the volume of the agglomerated particle.

The first term describes the coalescence of precipitates whose volumes are respectively $v-v'$ and v'. Merging upon contact, the two particles become one, the resulting volume equal to v. The second term describes the annihilation of the precipitates with volume of v through diffusion. After some manipulation Eq. (1) gives [33]:

$$\frac{dn}{\partial t} = -\frac{1}{2}\int_0^\infty \int_0^\infty W(v', v)\, f(v', t) f(v, t) dv' dv \quad (2)$$

where $n(t)$ is the number density of the particles and $n(t) = \int f(v, t)\ dv$.

To obtain the growth law for a particle with an average radius r_0, Eq. (2) can be simplified by considering $W(v', v) \approx \bar{W}$ that is the average volume of an agglomerated particle [34, 35]:

$$\frac{dn}{dt} = -\frac{1}{2}\bar{W} n(t)^2 \quad (3)$$

Eq. (3) shows that particle density in the agglomeration reaction decays with time. The solution to this equation is:

$$n(t) = \frac{n_0}{1 + \frac{1}{2} n_0 \bar{W}\ t} \quad (4)$$

where n_0 is the initial density of particles. Since agglomeration does not change the volume concentration of precipitates, $n_0 \bar{v}_0 = n(t)\overline{v}$(t) or:

$$\frac{4}{3}\pi \bar{r}_0^3 n_0 = \frac{4}{3}\pi \overline{r(t)}^3 n(t) \quad (5)$$

So, the change in the average particle radius is:

$$\overline{r(t)}^3 - \bar{r}_0^3 = \frac{1}{2} n_0 \bar{r}_0^3 \bar{W}\ t = K_{agg} t \quad (6)$$

Since the growth law is similar to that of the Ostwald ripening mechanism, it is possible to combine them, resulting in Eq. (7):

$$\overline{r(t)}^3 - \bar{r}_0^3 = (K_{LSW} + K_{agg}) t \quad (7)$$

3. Experimental Procedure

The material used in this study, AD730^{TM}, was supplied by Aubert & Duval Co. in the form of a forged square bar. A post forge heat treatment consisting in solutionizing at 1080°C for four hours followed by air cooling had also been conducted on the material. The chemical composition of the AD730^{TM} alloy used in this study is provided in Table 1. Three different solution treatment temperatures (1,080°C, 1,100°C and 1,110°C) were used in the investigation. These solutionizing temperatures were selected based on calculations using Thermo-calc® with the TCNI5 database and DTA results. The DTA was carried out using Diamond TG/DTA PerkinElmer with Pt crucible and a flowing Ar atmosphere. DTA samples were heated at the rate

of $1^{\circ}Cs^{-1}$ in order to replicate as close as possible the heating rate applied during the solutionizing process of γ′ particles.

Sample size for solution treatment trials was $5\times5\times5mm^3$. Holes of 1.5mm in diameter were drilled in the center of one face to a depth of 2.5mm before inserting a K-type thermocouple. All the tests were carried out on samples with thermocouples. Since thermal and thermomechanical processes are performed at various heating rates, two different heating rate ranges (low and high) were selected. The higher range used to simulate the dissolution process, the lower implemented to validate the model. For the high heating rate experiments, samples were heated from room temperature to $900^{\circ}C$ at a constant rate of $20^{\circ}Cs^{-1}$ and then from $900^{\circ}C$ to the target temperature at $1^{\circ}Cs^{-1}$. The heating cycle for the low heating rate experiments consisted of heating to $900^{\circ}C$ at $2^{\circ}Cs^{-1}$ and then from $900^{\circ}C$ to target temperature at $0.4^{\circ}Cs^{-1}$. The specimens were held for 1.5, 5, 15, 30, and 60 minutes, at the corresponding temperature followed by quenching in iced salt water at a rate of over $100^{\circ}Cs^{-1}$ in order to conserve the microstructure developed at high temperatures. For each test, the heating and cooling profiles were recorded by a computer aided electronic device using the attached thermocouple.

For microstructural studies, the samples were mounted and polished using standard metallographic techniques and etched using two different etchants. The first was composed of 170cc H_3PO_4, 10cc H_2SO_4 and 15gr Cro_3, the second a mixture of Regia water (2/3) and distilled water (1/3). After etching, the specimens' microstructures were observed using optical and Field Emission Gun Scanning Electron Microscopy (FEG-SEM). Characterization of the nanometric size particles and morphology of the precipitates were conducted using Hitachi SU70 SEM in the secondary electron (SE) mode. The back-scattered electron (BSE) images were recorded from polished cross sections by use of a backscattered electron detector attached to the SEM. Furthermore, distribution mappings of the different chemical elements constituting the specimen were obtained by Energy Dispersive Spectroscopy (EDS). Analyses were carried out at a microscopic scale using small and high magnification SEM images such as 2000, 50,000 and 100,000 magnifications to investigate γ′ morphology. The average dimensions and volume fractions of the γ′ precipitates were quantified using digitized images and ImageJ analysis software. The area of each particle was measured using the ImageJ software in view to measure γ′ phase size. The particle radius was then calculated as the radius of a circle whose surface area equaled that of the corresponding particle.

4. Results

4.1 Characteristics of the As-Received Material

FEG-SEM examination of the as-received AD730^{TM} material revealed that its microstructure consisted of γ matrix, primary γ′ precipitates, most of them present at the grain boundaries, intragranular secondary and tertiary γ′ particles, borides and two types of carbides (Figs. 1 and 2). The average size of the primary, secondary and tertiary γ′ were found to be 1.4 μm, 30 nm and 8 nm, respectively. Primary γ′ precipitates were oval and had irregular shapes while secondary and tertiary ones were either spherical or cuboidal. The average volume fractions of the primary, secondary and tertiary γ′ were measured and are 8%, 26%, and 3%, respectively.

MC carbides formed during solidification generally exhibit coarse, random, globular or blocky, and script morphologies and are located inside the γ matrix as well as at grain boundaries. The second type of carbides, $M_{23}C_6$, are observed mostly at grain boundaries in the form of films, globules, platelets, lamellae and cells. Borides are hard particles, blocky to half-moon appearance, that are observed at grain boundaries [2, 4, 36-38]. Fig. 2 presents an X-ray map of boron as well as the two former carbides. MC carbide and M_3B_2 boride phases mainly consist of Ti, Nb and Mo whilst the $M_{23}C_6$ phases contain significant amounts of Cr, Mo, and W. Out of all these elements, only Ti, Nb and Cr maps are shown in Fig. 2.

4.2 Thermo-calc® Simulations

The Thermo-calc® software is widely used for simulating phase transformations processes under equilibrium conditions. Fig. 3 shows a simulation of the amounts of phases, in moles, between 400 and 1400°C for the AD730^{TM} superalloy under equilibrium conditions on two different scales. On the first scale, phases like γ′, γ, liquid and σ are shown. The simulation results predict that the γ′ solvus, solidus, and liquidus temperatures are respectively 1090, 1220 and 1350°C. The secondary scale displays MC and $M_{23}C_6$ carbides, M_3B_2 borides and τ phases. The MC carbide is stable and does not dissolve until 1300°C.

It is well-known that, in Ni-based superalloys, the principal purpose of the homogenization process is to dissolve the irregular-shaped primary γ′ precipitates that are formed during the

casting process in view of fine particles re-precipitation during cooling [14]. Thus, from a theoretical point of view, the ideal temperature region for conducting the homogenizing of the investigated alloy would be between its γ′ solvus and solidus temperatures. This corresponds to a three- phase region composed of γ, MC carbide and M_3B_2 boride phases and in the temperature range of 1090-1220°C. Subsequently, the simulation results indicate that under equilibrium conditions, the percentage of γ′ phases, in moles, is 3% at 1080°C and no γ′ is present at 1100 and 1110°C.

4.3 DTA Experiments

Fig. 4 displays a DTA diagram obtained using a heating rate of $1^{\circ}Cs^{-1}$. Various endothermic peaks indicating the dissolution of γ′ at specific temperatures are revealed. Three peaks can be clearly distinguished from the heating curve: The first peak, Peak A, occurs around 615°C and shows that for a given phase volume fraction, some energy depicted by the area under the peak, is required for the transformation to be completed. This peak can correspond to the dissolution of tertiary (i.e. the finest) γ′ particles because equilibrium phase diagram calculated by Thermo-calc® software does not show any other phases with transformation temperature around 600°C. The second peak (Peak B), occurring around 800°C represents the dissolution of secondary γ′ particles, and the third peak is linked to primary γ′ dissolution and is around 1107°C (Peak C).

The above findings are in agreement with those of other researchers [10] who reported the temperature ranges of 600-650°C and 800-850°C for respective transformations of tertiary and secondary γ′ particles in Rene 88 DT superalloy, which contains almost the same volume fraction of γ′ as AD730™.

4.4 Dissolution Kinetics

Figs. 5 and 6 show the evolution of γ′ particles morphology and size after solution treatments at temperatures between 1080 and 1110°C. Heat treatment at 1080°C using a heating rate of $20^{\circ}Cs^{-1}$ results in the dissolution of all tertiary and secondary γ′ particles (Fig. 7 (b)) and the coarsening of primary γ′ (Figs. 5 (a), 6 and 7). As the temperature increases to 1100°C, tertiary, secondary

and small primary γ′ precipitates are dissolved. However, measurements of γ′ average size, shown in Fig. 6, indicate that the size of larger precipitates increases before final dissolution. These increases in particle sizes appear to be the result of two complementary processes: particles agglomeration (Figs.5 (a) and 5 (b)) and Ostwald ripening (Fig. 7). Measurements of γ′ size and volume fraction indicate that only particle dissolution is observed when increasing the solution temperature from 1080 to 1110°C. For instance, heat treatment at 1110°C for 15min leads to the complete dissolution of all the tertiary and secondary γ′ precipitates, forming initially 83% of the total γ′ content in the matrix. In addition, the primary γ′ average size is decreased from 1420 nm to 1150 nm and its volume fraction from 8% to 1%. It is also worth noting that the average volume fraction of γ′ reduces from 37% in the as received material to about 1% after solutionizing at 1110°C for 15 minutes.

Microstructural examinations of the samples heat treated at 1110°C revealed that 90% of γ′ particles are dissolved after a short holding time of 1.5 minutes (Fig. 5 (d)). After one hour, only 0.3% of initial γ′ remains. On the contrary, MC carbides average size and volume fraction show no change during heat treatment at 1110°C while $M_{23}C_6$ carbides are totally dissolved. Based on the above analyses, the γ′ solvus can be estimated to be about 1110°C for AD730™ with the high heating rate.

4.4.1 Dissolution Kinetics Model for a Single Precipitate

The dissolution of γ′ in Ni-based superalloys is a diffusion controlled process [8]. The following analytical model, based on the work of Whelan et al. [17], was applied to analyze this process in the AD730™ alloy.

The dissolution of a spherical precipitate under diffusion controlled conditions can be formulated as:

$$\frac{dr}{dt} = -\frac{kD}{2}\left[\frac{1}{r} + \frac{1}{\sqrt{\pi Dt}}\right] \tag{8}$$

The solution to Eq. (8) is:

$$r = r_0 - \frac{kDt}{2r_0} - \frac{k\sqrt{Dt}}{\sqrt{\pi}} \tag{9}$$

where r is the particle radius after 't' seconds, r_0 the initial precipitate radius, $k/2$ the supersaturation and D the solute interdiffusion coefficient in the matrix at temperature T. k is given by:

$$k = \frac{2(C_0 - C_{\mathrm{i}}^e)}{C_{\mathrm{p}}^e - C_{\mathrm{i}}^e} \tag{10}$$

where C_0 is the solute concentration in the matrix, C_{i}^e and C_{p}^e are equilibrium solute concentrations respectively at the precipitate/solid solution interface and in the precipitate.

Using the Thermo-calc® software, C_i and C_p values were calculated in the present investigation to estimate the coefficient k in Eq. (10). This value was determined to be 0.35 with Al and Ti considered as solutes.

The solute interdiffusion coefficient follows an Arrhenius type equation and is given by:

$$D = D_0 exp(\frac{-Q}{RT}) \tag{11}$$

where D_0 is the frequency factor, Q the activation energy, R the gas constant and T the absolute temperature.

Table II shows the calculated values of D for Al, Ti and Cr in a nickel matrix. As illustrated, D increases with the solutionizing temperature and therefore, according to Eq. (8), the dissolution rate should increase by 43% with a 30°C temperature increment starting from 1080°C.

The variation of precipitate radii versus dissolution time at 1110°C is plotted in Fig. 8 for three different particle sizes. The two biggest radii (1.4 and 0.5 μm) are representative of primary γ′, the smallest (0.2 μm) corresponds to secondary γ′. The dissolution rate is shown to increase from 1.46×10^{-3} μm .s^{-1} for primary γ′ to 5.02×10^{-3} μm .s^{-1} for secondary γ′, mainly due to their smaller sizes.

4.4.2 Dissolution Kinetics Model for Multiple Precipitates

A dissolution model based on Johnson-Mehl-Avrami-Kolmogorov (JMAK) [39] is proposed to study the precipitation evolution in AD730™. More specifically, the γ′ area fraction on various samples from different solution heat treatments is measured and used as a basis to estimate dissolution kinetics.

The γ′ area fraction ($F_{S\gamma'}$) can be written as a function of heat treatment time:

$$F_{S\gamma'} = F_{Slim} + F_1\, exp(\frac{-t}{t_1}) \quad (12)$$

where F_{Slim} is the γ′ area fraction at thermodynamic equilibrium, F_1 the difference between the γ′ area fraction at t=0 seconds and F_{Slim}, t_1 a constant dissolution time and F_{Slim} a material parameter. An optimization procedure was developed, using Origin and Matlab 2013, in order to find the values for the preceding factors for each solution heat treatment temperature. The procedure is based on nonlinear least-squares method and uses the Levenberg-Marquardt algorithm which was implemented in the optimization module. The routine searches for optimized parameter values.

The evolution of the γ′ area fraction as a function of the holding time for three different dissolution temperatures and the heating rate of 20°Cs^{-1} is presented in Fig. 9 (a). A decrease in area fraction of γ′ precipitates is observed as temperature or holding time increases. The different parameters of Eq. (12) were identified for each experimental condition allowing quantification of the dissolution kinetics.

The dissolution equations for each heat treatment temperature are given as follows:

$$F_{S\gamma'} = 5.83 + 31.16\, exp(\frac{-t}{0.69}) \quad \text{(For heat treatment at 1080°C)} \quad (13)$$

$$F_{S\gamma'} = 2.47 + 34.53\, exp(\frac{-t}{0.57}) \quad \text{(For heat treatment at 1100°C)} \quad (14)$$

$$F_{S\gamma'} = 1.08 + 35.92\, exp(\frac{-t}{0.54}) \quad \text{(For heat treatment at 1110°C)} \quad (15)$$

In order to quantify the differences in γ′ dissolution kinetics, a criterion, known as “settling time” or the time required to reach a given percentage of the equilibrium value was used [1]. This criterion is also used in the analysis of electronic systems and is shown schematically in Fig. 9 (b). In this research, a settling time of 95% was selected. As illustrated in Fig. 9 (b), T95% is the time needed for the γ′ volume fraction to satisfy the following condition:

$$0.95\mathrm{F}_{\mathrm{S}\gamma'}(\text{at } 60 \text{ min}) \leq \mathrm{F}_{\mathrm{S}\gamma'}(\text{at T95\%}) \leq 1.05\mathrm{F}_{\mathrm{S}\gamma'}(\text{at } 60 \text{ min}) \quad (16)$$

From the calculated $F_{S\gamma'}$ values and Arrhenius law, the activation energy (Q) for the dissolution of γ′ was calculated using the following equations:

$$k = \frac{dF_{s\gamma'}}{dt} = \frac{F_1}{t_1} exp(\frac{-t}{t_1}) \quad (17)$$

$$k = A\,exp(\frac{-Q}{RT_k}) \quad (18)$$

Table III shows the results for the kinetics of dissolution, k, and Q for different heat treatment temperatures at various holding times. As shown in Fig. 9 (a), although solutionizing starts with very high kinetics at the beginning due to the dissolution of large proportions of secondary γ′, it slows with time. After only 1.5 minutes, all ultra-fine γ′ precipitates, which make 83% of initial γ′ particles, are dissolved (see Fig. 7 (b)). The γ′ area fraction will reach 8%, 5%, and 3.3% respectively for 1080°C, 1100°C, and 1110°C, in comparison to 37% at room temperature.

The above findings are consistent with DTA results which showed that the dissolution temperature for ultrafine γ′ was lower than that of primary γ′ particles (Fig. 4). On the other hand, since primary γ′ particles are coarse and difficult to dissolve (Fig. 8), the activation energy increases from 204 kJ.mol^{-1} to 273 kJ.mol^{-1} demonstrating the impact of particle size on dissolution kinetics. Therefore, when holding times are longer than 1.5 minutes, dissolution becomes slower (Table III, Fig. 9 (a)). These results have revealed that the activation energy needed to dissolve γ′ varies during the dissolution process and that particle size evolution is an important consideration for accurate calculation of γ′ dissolution kinetics.

Bellot et al. [29] reported that γ′ particles in the AD730^{TM} alloy contain fractions of Al, Ti and Nb. So, the presence of Nb in secondary γ′ particles, which is not possible to be verified by EDS, has been proved using extraction replicas in the AD730^{TM} alloy [29]. Furthermore, Fig. 10 reveals schematically that primary γ′ precipitates contain higher contents of Al and Ti whilst secondary γ′ have lower Al and Ti and higher Co and Cr. Thus, in addition to particle size, chemical composition can also affect the dissolution rate in the multi precipitate model. Indeed, since the secondary γ′ particles in the as-received alloy were found to be small in size, their sizes increased using slower cooling rates (10°C/min) from 1110°C. In this way, as shown in Fig. 10, it was possible to obtain a qualitative estimate of the difference in the chemical composition between primary and secondary γ′ precipitates using EDS line map analysis. Therefore, it can be said that for primary γ′ particles, activation energy should be correlated mainly with those of Al and Ti while for secondary γ′, Al and Ti play a less important role in diffusion.

The activation energy values determined in the present investigation are in accordance with the reported activation energies for the dissolution of Al (269 kJ.mol^{-1}), Ti (272 kJ.mol^{-1}) [40, 41] and Nb (203 kJ.mol^{-1}) [42] elements in a nickel matrix. In other words, since Nb atoms have

lower activation energy than the other elements, their dissolution rate is higher and they dissolve first. By contrast, longer holding times increase the diffusion of Al and Ti atoms. The above results prove that the dissolution of γ′ precipitates is controlled mostly by the diffusion of Al, Ti and Nb in γ matrix. On the basis of the above calculations, average dissolution kinetics of -0.3 %.min^{-1} which shows decrease in volume fraction of γ′ precipitates as a function of time is obtained.

In addition to the well-known effects of temperature and holding time, heating and cooling rates also have significant effects on γ′ evolution in superalloys [43]. To address this aspect, a time-temperature dependent analytical method, proposed by Soucail and Bienvenu [43], was used in the present investigation to analyze the effect of a thermal cycle on γ′ evolution. In this model, equivalent holding time (t_e) is represented by the following equation:

$$t_e = \frac{RT_m^2}{Q}\left(\frac{1}{V_h} + \frac{1}{V_c}\right) + t_m \tag{19}$$

where T_m is the holding temperature, Q the activation energy for the dissolution of the γ′ phase, V_h and V_c respectively the heating and cooling rates, and t_m the holding time. t_e was calculated to be about $(32\ (\text{sec}) + t_m)$ at 1080 and 1100°C for low heating rates. Then, the γ′ surface fraction, $F_{S\gamma'}$, was calculated by substituting the obtained value into Eqs. (13) and (14). The calculated values of $F_{S\gamma'}$ for each temperature were validated through experimental data for low heating rate testing conditions. These values are presented in Fig. 11. The results indicate a good correlation between the calculated and measured data thereby confirming the validity of the proposed approach (Eqs. (13)-(15)).

4.5 Coarsening Kinetics Model

The experimental results reported in Fig. 5 indicated that γ′ coarsening takes place during the dissolution process. In order to determine the coarsening rate during this process, the Lifshitz, Slyozov, and Wagner (LSW) analytical model is modified to account for both Ostwald ripening and the agglomeration that occurs during the dissolution process. A linear relationship between heat treatment time and the cube of average precipitate size exists in the LSW model [18, 19]:

$$\bar{r}_t^3 - \bar{r}_0^3 = k_{LSW}t \tag{20}$$

where $\bar{r}_t$ is the average precipitate radius at time t, $\bar{r}_0$ the average precipitate radius at the beginning of coarsening, and k_{LSW} the coarsening rate constant. Umantsev, Olson and Philippe expanded the LSW theory to a multicomponent system (UO theory) [20, 21]. Since low mobility elements in a multicomponent alloy limit the kinetics of coarsening, for simplicity purposes, only Ti and Cr, which have the lowest mobilities, were considered for coarsening rate calculations. On this basis, the coarsening rate constant of γ′ precipitates, k_{UO}, is expressed as:

$$K_{UO} = \frac{8\sigma\Omega}{9RT[\frac{C_{Ti}^{\gamma}(1-K_{Ti})^2}{D_{Ti}} + \frac{C_{Cr}^{\gamma}(1-K_{Cr})^2}{D_{Cr}}]} \quad (21)$$

where σ is the interfacial free energy, Ω the molar volume of the γ′ precipitates, R the gas constant, T the heat treatment temperature, $D_i = D_0 \exp(\frac{-Q}{RT})$ the diffusion coefficient, C_i^{γ} the equilibrium concentration of the i th solute element in the γ matrix, and $K_i = \frac{C_i^{\gamma'}}{C_i^{\gamma}}$ the distribution coefficient of the i th solute element between the γ matrix and γ′ precipitates.

In the present investigation, the coarsening rate constant was determined and Eq. (20) was modified so that the contributions of both agglomeration and the Ostwald ripening processes were quantified. Furthermore, the flux from small to large particles is larger than expected with increasing volume fraction indicating that when the volume fraction of particles is not negligible, coarsening rate will increase [44]. The coarsening rate constant in Eq. (20) is therefore modified by $k(f_v)$, a precipitate volume fraction function [44, 45].

The results of FEG-SEM microscopy experiments (Figs. 5(a) and (b)) and reported simulations [23], however, demonstrate that the agglomeration mechanism cannot be excluded in the coarsening of Ni-based superalloys. It is reasonable to assume that particle growth follows a pattern similar to that of LSW during the agglomeration process as demonstrated in Eqs. (1) to (6). This assumption has also been used by Ratke for modeling particle coarsening through coagulation [34, 35].

Combining Eq. (6) and Eq. (20), and considering that $k_{Coarsening}$ is dependent on the γ′ volume fraction, the following equation is obtained:

$$r_t^3 - r_0^3 = k(f_v)(k_{UO} + k_{agg.})t \quad (22)$$

Therefore, agglomeration and Ostwald ripening coarsening follow the same growth law for average γ′ particle size with different rate constants.

The coarsening rate can be written as Eq. (23) considering that C'^{γ}_{i} is a temperature dependent, and being different of $k(f_v)$ values for various γ′ volume fractions:

$$k_{Coarsening} = \frac{A_0 k(f_v)}{(D_{0Ti} C'^{\gamma}_{Cr} + D_{0Cr} C'^{\gamma}_{Ti})T} \times exp(\frac{-Q}{RT}) \quad (23)$$

where $C'^{\gamma}_{Cr} = C^{\gamma}_{Cr}(1 - k_{Cr})^2$ and $C'^{\gamma}_{Ti} = C^{\gamma}_{Ti}(1 - k_{Ti})^2$.

The value of $k(f_v)$ was found by Ardell [44], Voorhees and Enomoto [45] for different volume fractions of precipitates. Voorhees and Enomoto reanalyzed the model both analytically and numerically showing coarsening rate increases with the volume fraction but at a slower rate than first suggested by Ardell [44]. Using the above analysis, the value of $k(f_v)$ for the present investigation is considered to be 1.2 and 1.3 for 1100°C and 1080°C heat treatment temperatures, respectively.

The activation energy Q for γ′ dissolution in AD730™ was calculated to be 273 kJ.mol^{-1} from the slope of the plot of Lnk versus $1/T$, with k representing dissolution kinetics. The calculated value is close to reported activation energies for the diffusion of either Ti (272 kJ.mol^{-1}) or that of Cr in a Ni matrix (286 kJ.mol^{-1}) [40]. Values for D_{0i} are given in Table II. C'^{γ}_{i} values were determined for different elements of solute in a γ matrix at various heat treatment temperatures by Thermo-calc® software. Fig. 12 shows the composition of solute elements in the γ matrix and γ′ precipitates at different temperatures. The coarsening kinetics of γ′ particles in AD730™ can be predicted using Eqs. (20), (21) and (23):

$$r_t^3 - r_0^3 = \frac{2.23 \times 10^{-13}\, k(f_v)}{(D_{0Ti} C'^{\gamma}_{Cr} + D_{0Cr} C'^{\gamma}_{Ti})T} exp(\frac{-273000}{RT})t \quad (24)$$

According to the data presented in Fig. 12, the mass percentages of Ti and Cr in the γ matrix were determined to be 3.2% and 16.1% respectively. Furthermore, k_{Ti} and k_{Cr} were calculated to be 3.34 and 0.09 respectively. Since the fluctuation of C'^{γ}_{i} is negligible for temperatures around 1080°C and 1100°C, using previous data and Eq. (24), kinetics of γ′ coarsening for this alloy at these temperatures can be summarized by:

$$r_t^3 - r_0^3 = \frac{1.53 \times 10^{-11}\, k(f_v)}{T} exp(\frac{-273000}{RT})t \quad (25)$$

5. Discussion

5.1 γ′ Precipitate Size Evolution after Short Exposure Time

As shown in Fig. 6, γ′ size decreases continuously for the first 1.5 minutes for all heat treatment temperatures (i.e. the dissolution process is dominant). However, the dissolution rate is higher at 1100 and 1110°C than that observed at 1080°C. These findings are in agreement with the calculated values based on the diffusion coefficients (Table II) and Eq. (8).

Fig. 13 regroups the evolution of the primary γ′ size distribution during dissolution for three different temperatures below and around the AD730™ γ′ solvus. In all cases, the peak was observed to shift to smaller precipitate size after 1.5 minutes. In the case of 1080°C, only size reduction of γ′ occurs and particle disappearance is not observed while for the other temperatures, only few γ′ disappear. The previous analysis confirms that for the investigated conditions average particle size reduces with time and is mostly controlled by γ′ size reduction up to 1.5 minutes (Fig. 6). Moreover, as shown in Fig. 8, the dissolution rate of the large precipitates is slower compared to that of fine particles.

So, it is predicted that primary (large) γ′ particles also dissolve slower than secondary (fine) γ′ in multiple particles dissolution process because more solutes are required to diffuse from large particles toward the matrix. Consequently, soft impingement may take place. In addition, when small particles dissolve, large precipitates grow due to the Ostwald ripening effect. Moreover, primary γ′ particles have higher amounts of Al and Ti and lower contents of Co and Cr than those of secondary γ′ (Fig. 10) which slows down further the dissolution process. Thus, the combination of the soft impingement process, the coarsening processes and chemical composition can probably lead to a deceleration of the dissolution of the large γ′ particles.

5.2 γ′ Precipitate Size Evolution after Longer Holding Times

As shown in Fig. 6, γ′ coarsening is observed for 1080°C and 1100°C solution heat treated samples and for holding times superior to 1.5 minutes whereas dissolution dominates for the 1110°C heat treated samples. It was shown that after solution heat treatments at 1080°C and 1100°C, *agglomeration* of the primary γ′ particles (Figs. 5(a) and 5(b)), and their *coarsening* at

the expense of secondary or tertiary γ′ (Fig. 7) take place. Fig. 14 shows an illustrative example of the coalescence of two γ′ particles through a diffuse necking process. Agglomeration is seen to start by neck formation between two neighboring particles which is consistent with the predictions for multicomponent Ni (Al, Cr) alloys [23]. It must be noted that the coalescence process includes the overlapping of precipitates diffusion fields followed by neck formation. Finally, fast diffusion along the precipitate-matrix interface leads to its migration and precipitates coalescence [23].

In addition to neck formation, solute absorption from the matrix could be an additional factor influencing γ′ coarsening during solution heat treatment. The solute absorption process is characterized by the formation of denuded zones around primary γ′ particles [21]. The results obtained in the present investigation confirm the occurrence of a solute absorption process in the AD730^{TM} alloy. An illustrative example is shown in Fig. 7 (b) where denuded zones from secondary and tertiary γ′ can be observed around primary γ′ in 1080°C solution treated samples for 5 minutes. As reported in the section above, all tertiary γ′ precipitates were dissolved after a 1.5 minute holding time for any of the three selected SHT temperatures. The dissolved fine particles could provide the necessary solutes which could migrate to the larger particles, thus increase the size of the larger particles.

Coarsening continues up to 15 minutes holding time for SHT at 1100°C and 60 minutes for 1080°C. As particle size measurements did not indicate significant changes between 15 and 30 minute holding times at 1080 and 1100°C (Fig. 6), comparisons were made for the 30 minute holding time condition only. Fig. 13 shows that for 1080°C SHT, precipitate size distribution peak after a 30 minute holding time shifts to the larger particle size of 1.24 μm in comparison to 1.15 μm for the 1.5 minute holding time. For 1100°C SHT, the peak at the 30 minute holding time also shifts to 1.05 μm compared to 950 nm for 1.5 minute holding time. However, the number of particles decreases from 15 to 10 for 1080°C and from 10 to 4 for 1100°C SHT. These findings confirm the occurrence of coarsening for holding times superior to 1.5 minutes due to the coalescence and agglomeration of γ′ particles (Figs. 5 and 7). Average γ′ size is therefore controlled by particle disappearance and solute diffusion between adjacent particles.

5.2.1 Determination of the Coarsening Rate

Using Eq. (22) and the experimental data provided in Fig. 6, the total coarsening rate constant (i.e. $k(f_v)(k_{UO} + k_{agg.})$) was calculated to be 3.24×10^{-23} m^3s^{-1} for SHT at 1080°C and 6.31×10^{-23} m^3s^{-1} for SHT at 1100°C. The determined values indicate that γ′ precipitates coarsen about two times faster for a solution temperature at 1100°C in comparison to 1080°C. The value of the agglomeration coefficient $k_{agg.}$ was also determined to be 3.15×10^{-23} m^3s^{-1} and 6.13×10^{-23} m^3s^{-1} respectively, for heat treatments at 1080°C and 1100°C. The results indicate that agglomeration has the most important contribution (97%) to the coarsening process for SHT temperatures of 1080 and 1100°C; while the contribution of the Ostwald ripening process is only very minor (3%).

The fraction of agglomerated γ′ particles (ξ) is obtained by:

$$\xi = \frac{N_{ppt.}^{Agg.}}{N_{ppt.}^{Tot.}} \tag{26}$$

where $N_{ppt.}^{Agg.}$ is the number of agglomerated γ′ particles and $N_{ppt.}^{Tot.}$ the total number of γ′ particles in the analyzed surface. The values of ξ for heat treatments at 1100°C shown in Fig. 15 indicate that the amount of agglomeration first increases for longer heat treatment times before reaching a peak value for 15 minutes holding time and then decreases as the time increases.

On the other hand, agglomeration monotonically increases as the heat treatment time at 1080°C increases. These trends are similar to the ones observed for the evolution of average γ′ particle size with time, as previously reported in Fig. 6, indicating that coarsening is mainly dominated by the agglomeration of the precipitates. Furthermore, Fig. 15 reveals that the coarsening rate for 1100°C is higher than that of 1080°C, correlating with the previous finding of a higher value (almost twice) for $k_{agg.}$ at 1100°C in comparison to 1080°C.

As a result, it is concluded that both mechanisms, agglomeration and Ostwald ripening, govern γ′ size evolution during the heat treatment process of the AD730™ Ni-based superalloy. However, it appears that the Ostwald ripening contribution is negligible, affirming agglomeration is the dominant coarsening mechanism for short heat treatments at subsolvus or around solvus temperatures.

The evolution of the cubed of the precipitate radius, $\bar{r}^3$, as a function of holding time, t, is plotted in Fig. 16 for heating conditions of 1080 and 1100°C. A linear relationship was identified (R^2 >0.93), suggesting that particles growth kinetics follow a cube power law and are consequently diffusion controlled. In addition, the slope of the linear regression increases for higher solution temperatures indicating faster coarsening rates. This further confirms the obtained values of $k(f_v)(k_{UO} + k_{agg.})$ for 1080 and 1100°C and the results obtained from Fig. 15 in which the coarsening rate is higher for heat treatments at 1100°C.

5.2.2 Application to Aging Heat Treatments

Using Eq. (24), the evolution of γ′ average size after various aging times for different heat treatment temperatures can be predicted. Fig. 17 illustrates this evolution for aging heat treatments at 700°C, 750°C and 800°C. Monajati et al. reported that γ′ particles above 200nm in size play a smaller role in the hardness increment for Udimet 720 [9]. It has also been reported that in Ni-based superalloys, the achievable optimum hardening is directly related to an optimal γ′ particle size. For example, for PE16 and Nimonic 105, the optimum diameter was respectively found to be in the range of 26-30 nm and 55-85 nm [46]. Hence, the data in Fig. 17 can be practically used to design aging heat treatment schedules for the AD730™ superalloy in order to reach the desired γ′ particle size. This was applied in the current investigation for average secondary γ′ particle size of the as-received material which was 30nm.

On the basis of the above findings, Eq. (24) and Fig. 17, an aging heat treatment at 750°C for 8 hours would be necessary to reach a mean diameter of 40nm. In order to achieve precipitate sizes of 60 nm, an 8 hour holding at 800°C would be required. Devaux et al. [47] carried out aging heat treatment at 750°C for 8 hours and reached an average particle size of 37nm. This value is very close (about 7% difference) to the predicted value by the model proposed in this investigation.

The proposed treatment is also very close to the one reported by the former authors who used 730°C for 8 hours in order to achieve the best compromise between creep and tensile properties [47]. Therefore, Eq. (24) and Fig. 17 can be used as a very efficient tool for determining desired γ′ size for specific applications such as aging.

5.3 γ′ Precipitate Dissolution Mechanisms

As Figs. 5 and 6 show, only dissolution is observed for heat treatments at 1110°C. Under these conditions, fine precipitates are completely dissolved during the early stages of heat treatment. Average particle size is therefore totally controlled by primary γ′ size reduction for the entire holding time. Fig. 13 shows a shift of particle size peaks to lower values and a reduction in the number of particles for all holding times. γ′ size peak reaches 800nm, from a starting value of 1.35 μm in as-received condition, after a 30 minute holding time at 1110°C. The number of particles decreases by 53%. Complete dissolution of primary γ′ particles occurs at 1110°C for a holding time of 60 minutes and with the high heating rate.

Interestingly, the number of particles is increased by 50% for 1100°C SHT and a holding time of 60 minutes, although γ′ size peak shifts to smaller values of 950 nm from a starting value of 1.05 μm in comparison with a 30 minute holding time at1100°C. This confirms that primary γ′ particles break into small pieces or split until their complete dissolution occurs (Fig. 18).

Several dissolution patterns were observed depending on the SHT temperature. As shown in Fig. 18, splitting of the γ′ particles in which two or more particles with parallel interfaces are created and dissolving from the center, corner and in the form of layers of γ and γ′ are observed. Similar behavior was also reported for other Ni-based superalloys [46]. The results of the present investigation are in agreement with the theoretical model of Doi [48] and finite element model of Hazotte [49] in which they stated that above a certain lattice misfit value and consequently certain strain energy, particles split to create precipitates with parallel interfaces.

The results obtained based on the analytical model for single particle dissolution illustrate that secondary and primary γ′ with diameters of 200 nm and 1.4 μm dissolve completely after respectively 12 seconds and 6 minutes. However, experimental results indicated that, a 15 minute holding at 1110°C is required to reach a 1% γ′ volume fraction and 60 minutes in order to reach 0.3 % γ′. As the analytical solution is limited to single precipitate dissolution in a matrix, it does not consider the impingement of diffusion fields of neighboring particles nor precipitate size distribution during the dissolution process. This probably explains the underestimated dissolution times obtained by using the single particle model. The proposed multi-particle model however, has a relatively better prediction of γ′ dissolution kinetics as illustrated in Fig. 9 (a) and Eqs. (13)-(15).

Figs. 19 (a) and 19 (b) compare precipitate size distribution for the three selected SHT temperatures for holding times of 30 and 60 minutes, respectively. It can be seen that, the peak shifts to smaller particle sizes for higher temperatures and time values suggesting particle dissolution is dominant during heat treatments at 1100 and 1110°C for the above holding times. Furthermore, the number of particles for a heat treatment at 1110°C is superior by 75% in comparison to that of 1100°C for 30 minutes holding times. This indicates the breaking and splitting of larger particles into smaller ones (Fig. 19).

The observations are in agreement with phase field simulations reported previously by Wang et al. [13] and confirm the simulation results concerning the occurrence of coarsening before final dissolution. It is important to note that the results obtained in this research can be directly applied to thermal or thermomechanical processes characterized by very short or long processing times. For example, the findings can be applied to analyze the Linear Friction Welding (LFW), an emerging joining process in aerospace industry [50] in which the joining cycle is completed in less than 30 seconds. Based on the data presented in Fig. 6, only dissolution is dominant in heating cycles less than 1.5 minutes. γ′ evolution and dissolution kinetics can therefore be modeled from the dissolution equations allowing for rapid optimization of the LFW process parameters. Similarly, for some thermal processes such as aging, post weld heat treatments and creep in which the process time is long, coarsening equations can be applied.

6. Summary and Conclusions

This study represents a detailed investigation of the dissolution and coarsening mechanisms and kinetics of γ′ precipitates during solution treatment in the newly developed AD730™ Ni-based superalloy. The findings are summarized as follows:

1-Evidence of various dissolution temperatures for different size distributions of γ′ were observed by DTA investigation. Three methods including DTA, Thermo-calc®, and heat treatments via microstructure observations were used to determine the dissolution temperature of the primary γ′ particles. The solvus temperatures of primary, secondary and tertiary γ′ were determined to be 1110°C, 800°C, and 615°C respectively.

2- Dissolution kinetics and coarsening models are proposed to predict γ′ volume fraction and its average size at various heat treatment temperatures. The results from the proposed models and

FEG-SEM observations indicate that before complete dissolution, coarsening through agglomeration and Ostwald ripening occurs when short holding times at subsolvus temperatures are used. It was also found that not just the average size, but the size distribution of the γ′ phase plays a critical role in microstructural evolution in the dissolution and coarsening processes.

3- The activation energy during the dissolution process of the AD730^{TM} alloy was determined during this investigation. This value varies throughout the heat treatment cycle; 204 kJ.mol^{-1} up until 1.5minutes, increasing to 273 kJ.mol^{-1}after that. The dissolution of γ′ precipitates is concluded to be mostly controlled by the diffusion of Al, Ti and Nb in the γ matrix.

4- The contribution to coarsening from agglomeration and Ostwald ripening were quantified for temperature ranges from 1080°C to 1100°C. In the case of the AD730^{TM} superalloy, agglomeration contributes for 97% compared to only 3% for the Ostwald ripening mechanism.

5- It is demonstrated that the early stage of agglomeration is created by neck formation between two neighboring particles. Splitting and breaking of the larger γ′ particles into smaller ones and dissolution from the center of the particles can be identified as mechanisms of γ′ dissolution.

6- A single particle analytical model was used to determine dissolution kinetics and a multi-particle semi-analytical dissolution model was proposed to quantify and predict dissolution kinetics. The models were validated by experiments. The comparison of single and multi-particle models indicated that the proposed multi-particle model has a relatively better prediction of γ′ dissolution kinetics.

7. Acknowledgements

The financial support from the Natural Sciences and Engineering Research Council (NSERC) of Canada in the form of a Discovery Grant is gratefully acknowledged. The authors express appreciation to Aubert & Duval Co. and to Dr. Alexandre Devaux for providing AD730^{TM} samples and for invaluable discussions.

Appendix A: Analytical Solution to the Non-Linear Differential Equation: Eq. (8)

Eq. (8) is used for dissolution of a spherical precipitate:

$$\frac{dr}{dt} = -\frac{kD}{2}\left[\frac{1}{r} + \frac{1}{\sqrt{\pi Dt}}\right]$$

To integrate Eq. (8) assuming:

$$a = \frac{2D(C_0 - C_\gamma^e)}{C_{\gamma\prime}^e - C_\gamma^e};\ b = \frac{\sqrt{\frac{D}{\pi}}(C_0 - C_\gamma^e)}{C_{\gamma\prime}^e - C_\gamma^e};\ p = \frac{b}{a};\ y = \frac{R}{R_0};\ \tau = \frac{a^2 t}{{R_0}^2} \tag{A1}$$

Eq. (8) then becomes:

$$\frac{dy}{d\tau} = -\frac{1}{2y} - \frac{p}{\sqrt{\tau}} \tag{A2}$$

Eq. (A2) can be integrated by substitution $y^2 = w^2\tau$. Therefore, the following implicit relation for y as a function of τ is obtained.

$$\ln\left(y^2 + 2p\sqrt{\tau}y + \tau\right) = -\frac{2p}{\sqrt{1-p^2}}\ tan^{-1}\left(\frac{\sqrt{1-p^2}}{\left({}^{y}/_{\sqrt{\tau}}\right) + p}\right) \tag{A3}$$

Thus, Eq. (8) at short times is integrated approximately to give an analytical solution. Hence the answer for this assumption is:

$$y = 1 - \tfrac{1}{2}\tau - 2p\sqrt{\tau} \tag{A4}$$

This gives the solution of:

$$r = r_0 - \frac{kDt}{2r_0} - \frac{k\sqrt{Dt}}{\sqrt{\pi}}$$

References

[1] Giraud R, Hervier Z, Cormier J, St Martin G, Hamon F, Milhet X, Mendez J. Metall Mater Trans A 2013; 44A:131.

[2] Shahriari D, Sadeghi MH, Akbarzadeh A, Cheraghzadeh M. Int. J. Adv Manuf Technol 2009; 45(9–10): 841.

[3] Cormier J, Milhet X and Mendez J. J Mat Sci 2007; 42:7780.

[4] Shahriari D, Sadeghi MH, Akbarzadeh A. Mater Manuf Processes 2009; 24:559.

[5] Payton E.J. Superalloys 2008, ed. by R.C. Reed : 975, Warrendale, PA, 2008, The Minerals, Metals & Materials Society 43: 60.

[6] Cormier J, Cailletaud G. Mater Sci Eng A 2010;527:6300.

[7] le Graverend JB , Cormier J, Gallerneau F, Villechaise P, Kruch S, Mendez J. Int J Plasticity 2014;59: 55.

[8] Fuchs GE. Mater Sci Eng A 2001; 300:52.

[9] Monajati H, Jahazi M, Bahrami R ,Yue S. Mater Sci Eng A 2004;373:286.

[10] Singh ARP, Nag S, Chattopadhyay S, Ren Y, Tiley J, Viswanathan GB, Fraser HL, Banerjee R. Acta Mater 2013;61:280.

[11] Wen YH, Wang B, Simmons JP, Wang Y. Acta Mater 2006;54: 2087.

[12] Radis R, Schaffer M, Albu M, Kothleitner G, Polt P, Kozeschnik E. Acta Mater 2009;57:5739

[13] Wang G, Xu DS, Ma N, Zhou N, Payton EJ, Yang R., Mills MJ, Wang Y. Acta Mater 2009;57: 316.

[14] Semiatin SL, Kramb RC, Turner RE, Zhang F, Antony MM. Scripta Mater 2004;51:491.

[15] Ojo OA, Richards NL, Chaturvedi MC. J Mater Sci 2004; 39:7401.

[16] Thomas G, Whelan MJ. Philos Mag. 1961;6:1103.

[17] Whelan MJ. Met Sci J 1969;3:95.

[18] Lifshitz IM, Slyozov VV. J Phys Chem Solids 1961;19(1/2):35.

[19] Wagner C. Z Elektrochem 1961;65:581.

[20] Umantsev A, Olson GB. Scripta Metall Mater 1993;29(8):1135.

[21] Philippe T, Voorhees PW. Acta Mater 2013;61:4237.

[22] Wang T, Sheng G, Liu ZK, Chen LQ. Acta Mater 2008;56:5544.

[23] Mao Z, Sudbrack CK, Yoon K, Martin G, Seidman DN. Nat Mater 2007;6:210.

[24] Ferro P. Acta Mater 2013;61:3141.

[25] Kovacevic I, Sarler B. Mater Sci Eng A 2005;413–414:423.

[26] Ferro P, Bonollo F. Metall Mater Trans A 2012;43:1109.

[27] Lee ES, Kim YG. Acta Metall Mater 1990;38:1669.
[28] Lee ES, Kim YG. Acta Metall Mater 1990;38:1677.
[29] Bellot C, Lamesle P. J Alloys Compd 2013;570:100.
[30] Devaux A, Picque B, Gervais MF, Georges E, Poulain T, Heritier P. TMS Superalloys 2012: 911.
[31] Masoumi F, Jahazi M Cormier J, Shahriari D. MATEC Web of Conferences 2014;14:13005.
[32] Smoluchowski MV. Phys. Z. 1916;17(23):557; Phys. Z. 1916;17(23):585.
[33] Thompson PD. Proc. Int Conf on Cloud Physics1968:115.
[34] Ratke L. J Colloid Interface Sci 1987;119(2):391.
[35] Ratke L. Mater Sci Eng A 1995;203:399.
[36] Sajjadi SA, Zebarjad SM, Guthrie RIL, Isac M. J Mater Proc Technol 2006;175:376.
[37] Safari J, Nategh S. J Mater Proc Technol 2006;176:240.
[38] Siddall RJ, Eggar JW. Mater Sci Technol 1986;2:728.
[39] Avrami M. J Chem Phys 1941;9:177.
[40] Campbell CE, Boettinger WJ, Kattner UR. Acta Mater 2002;50:775.
[41] Baldan A. J Mater Sci 2002;37:2379.
[42] Patil RV, Kale GB. J Nucl Mater 1996;230:57.
[43] Soucail M, Bienvenu Y. Mater Sci Eng A 1996; 220:215.
[44] Laughlin DE, Hono K. Physical Metallurgy, vol. I. 5th ed. Elsevier; 2014.
[45] Voorhees PW, Glicksman ME. Acta Met 1984;32:2013.
[46] Reed RC. The Superalloys: Fundamentals and Applications. New York: Cambridge University Press; 2006.
[47] Devaux A, Helstroffer A, Cormier J, Villechaise P, Douin J, Hantcherli M, Pettinari-Sturmel F. TMS Superalloys 2014: 521.
[48] Doi M, Miyazaki T. TMS Superalloys 1992: 537.
[49] Hazotte A, Grosdidier T, Denis S. Scripta Mater 1996;34 Issue4:601.
[50] Mary C, Jahazi M. Advanced Material Research 2007;15–17:357.

List of Tables

Table 1. Chemical composition of AD730^{TM} (wt%) [30]

Ni	Fe	Co	Cr	Mo	W	Al	Ti	Nb	B	C	Zr
Base	4	8.5	15.7	3.1	2.7	2.25	3.4	1.1	0.01	0.015	0.03

Table II. Activation energies Q , frequency factors D_o [40] and calculated D for the diffusion of aluminium, titanium and chromium in nickel

Element	D_0 (m^2s^{-1})	Q (KJ $mole^{-1}$)	T($^{\circ}$K)	*Calculated D (m^2s^{-1})
Al	2.94×10^{-4}	269	1353	1.2×10^{-14}
			1373	1.7×10^{-14}
			1383	2.1×10^{-14}
Ti	4.1×10^{-4}	275	1353	9.9×10^{-15}
			1373	1×10^{-14}
			1383	2×10^{-14}
Cr	5.2×10^{-4}	289	1353	3.6×10^{-15}
			1373	5.2×10^{-15}
			1383	6.3×10^{-15}

*This work

Table III. Dissolution kinetics and activation energies for various solution treatments

t (min)	T ($^{\circ}$K)	K (%.min^{-1})	Q (kJ.mol^{-1})
0-1.5	1353	-0.45159	204
	1373	-0.60042	
	1383	-0.66565	
1.5-5	1353	-0.0247	273
	1373	-0.03912	
	1383	-0.04066	

List of Figures

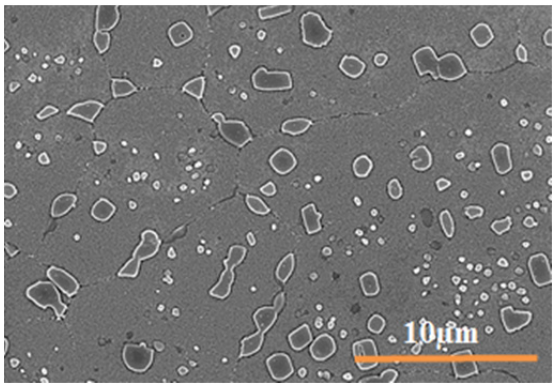

(a)

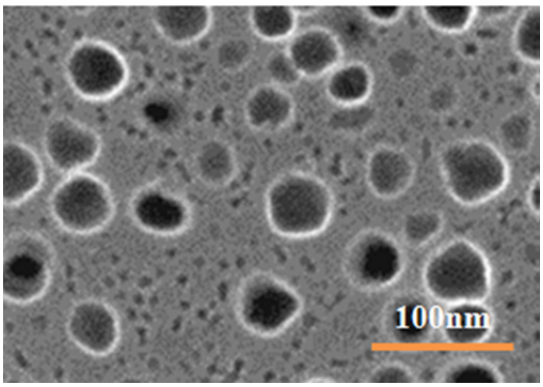

(b)

Fig. 1. SEM microstructure of the as-received AD730^{TM} superalloy showing a) primary γ′ b) secondary and tertiary γ′

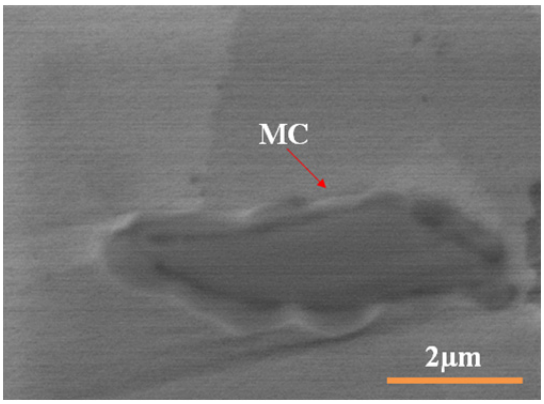

Back-scattered electron image of MC carbide

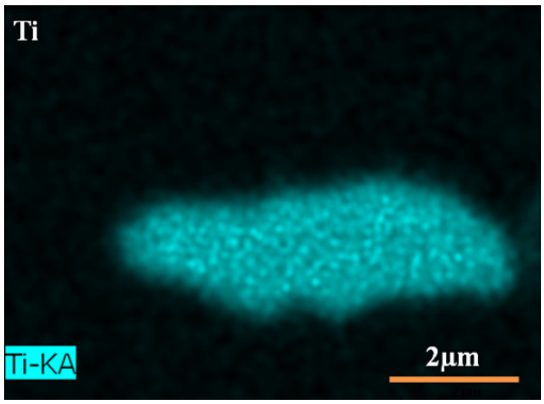

Ti-

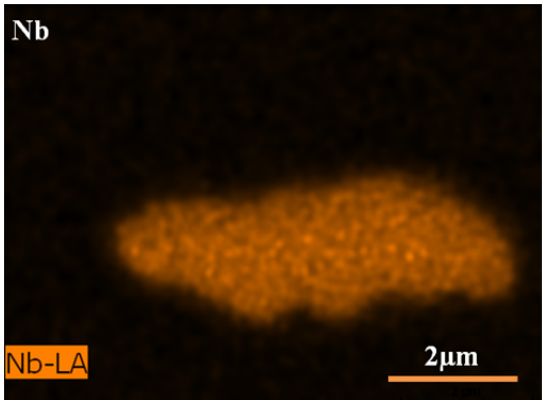

Nb-

(a)

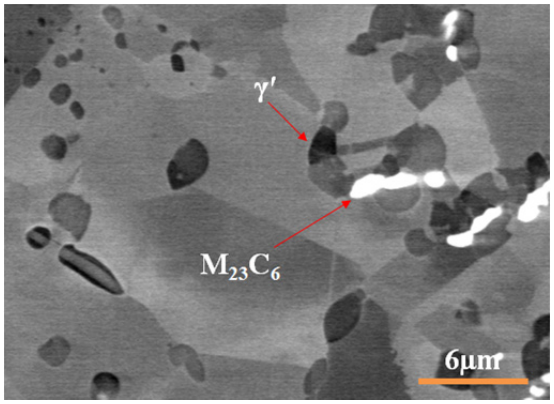

Back-scattered electron image of $M_{23}C_6$ carbides

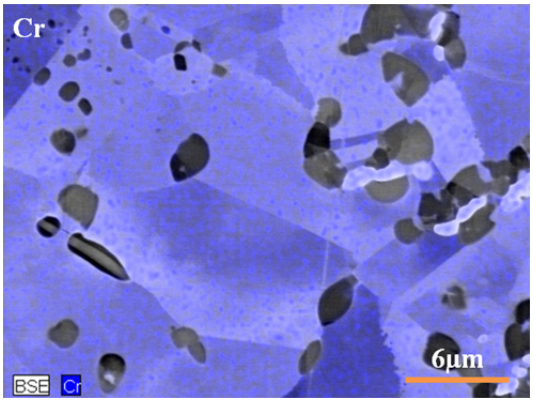

Cr-

(b)

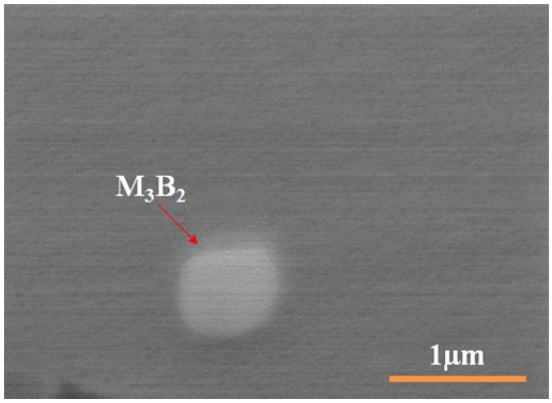

Back-scattered electron image of M_3B_2 boride

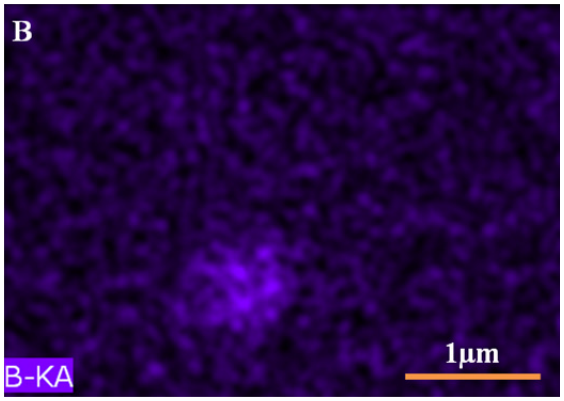

B-

(c)

Fig. 2. BSE/EDS X- ray maps of the (a) MC carbide mainly consisting of Ti, Nb (b) $M_{23}C_6$ carbides mainly consisting of Cr (c) M_3B_2 boride

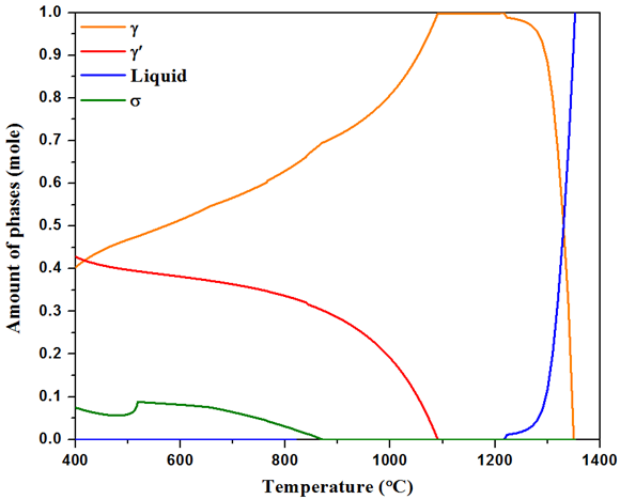

(a)

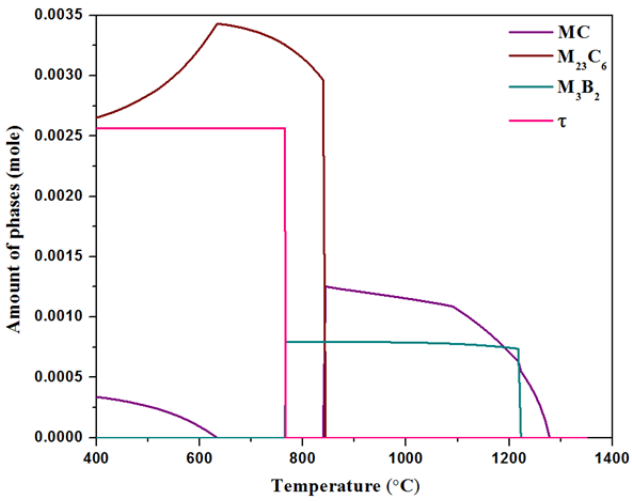

(b)

Fig. 3. (a) and (b) Calculated equilibrium phase diagram of AD730^{TM} superalloy representing the amounts of all phases between 400 and 1400°C

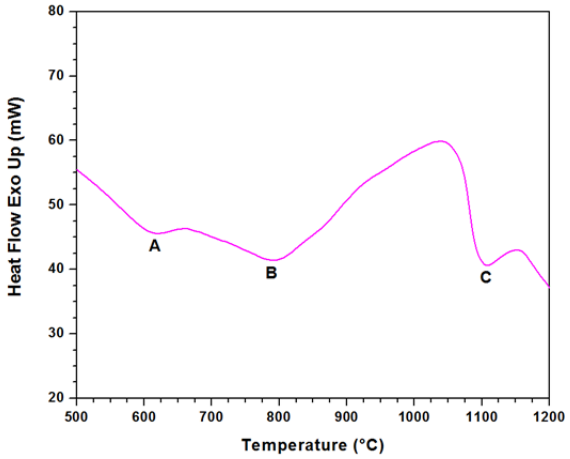

Fig. 4. DTA curve at the 1°Cs^{-1} heating rate, showing three endothermic reactions that occur during heating indicating tertiary (Peak A), secondary (Peak B) and primary γ′ (Peak C) dissolution temperatures

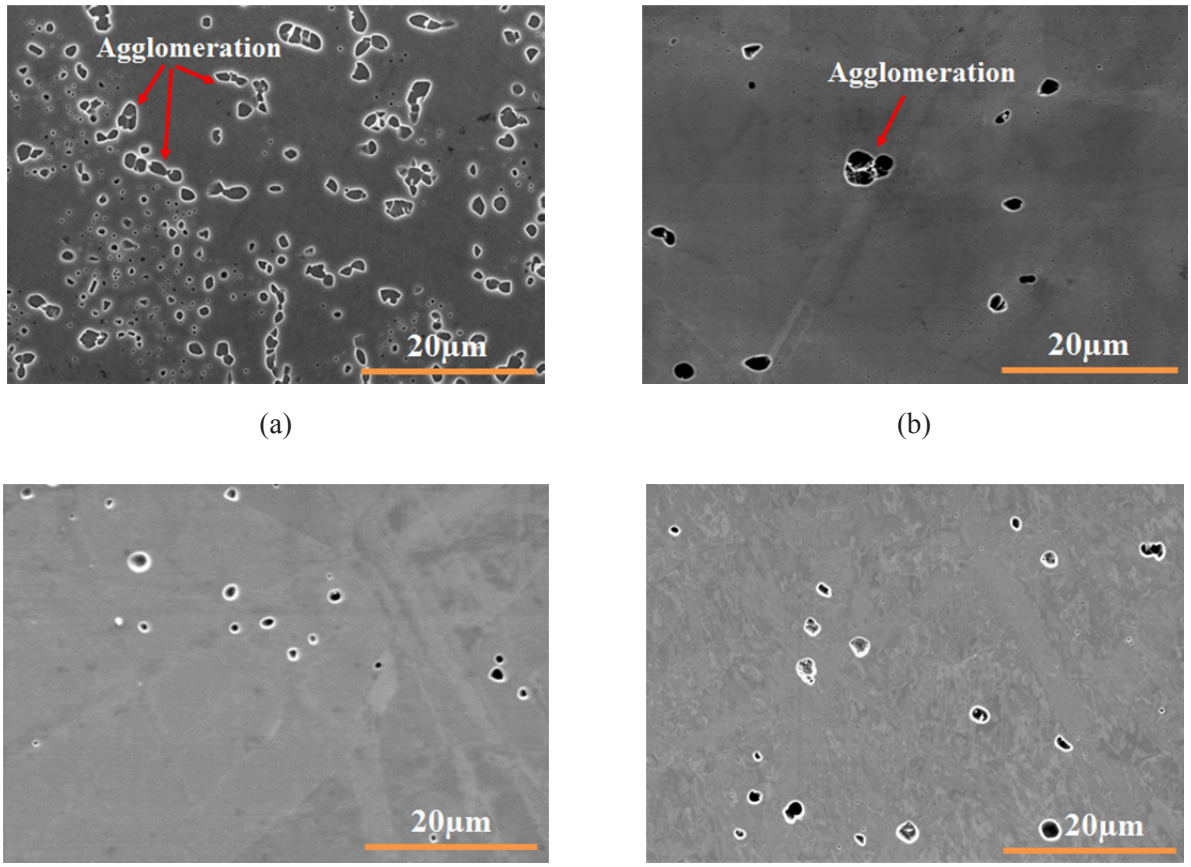

Fig. 5. Microstructure of solution treated samples at (a) 1080°C for 15min and (b) 1100°C for 15min, showing the occurrence of γ′ particles agglomeration (c) 1110°C for 15min and (d) 1110°C for 1.5min, showing γ′ particles' dissolution

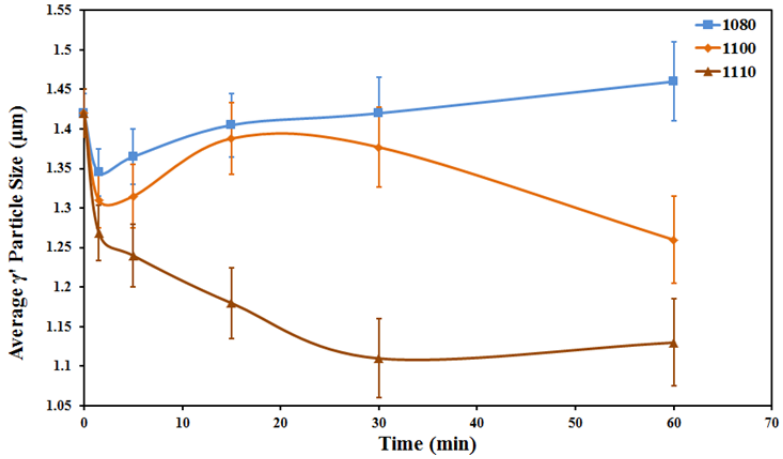

Fig. 6. Evolution of average γ′ particle size as a function of time at 1080, 1100 and1110°C

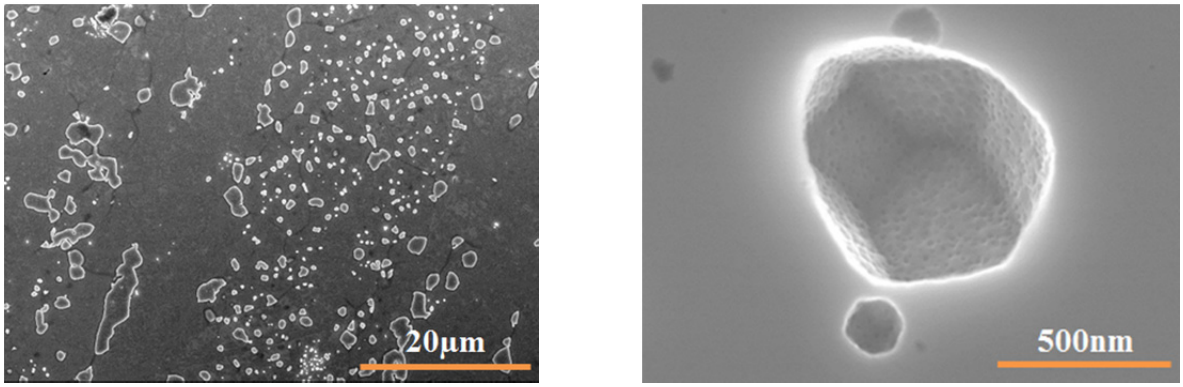

(a) (b)

Fig. 7. Denuded zones from the small precipitates around primary γ′ particles at 1080°C for 5 minutes at (a) lower magnification (b) higher magnification

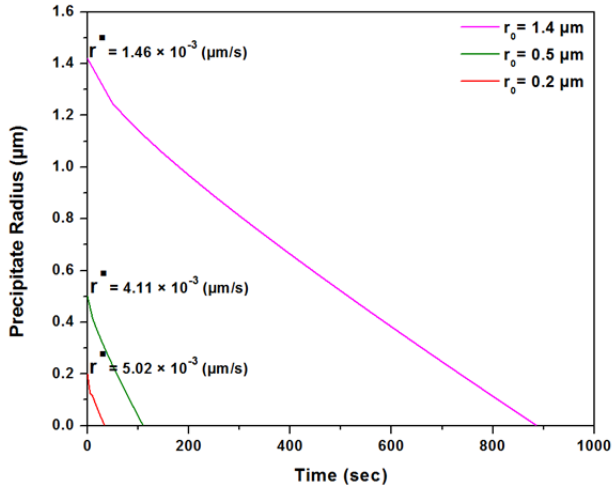

Fig. 8. Comparison of the single γ′ precipitate dissolution kinetics at different sizes at 1110°C indicating the influence of particle size on dissolution rate

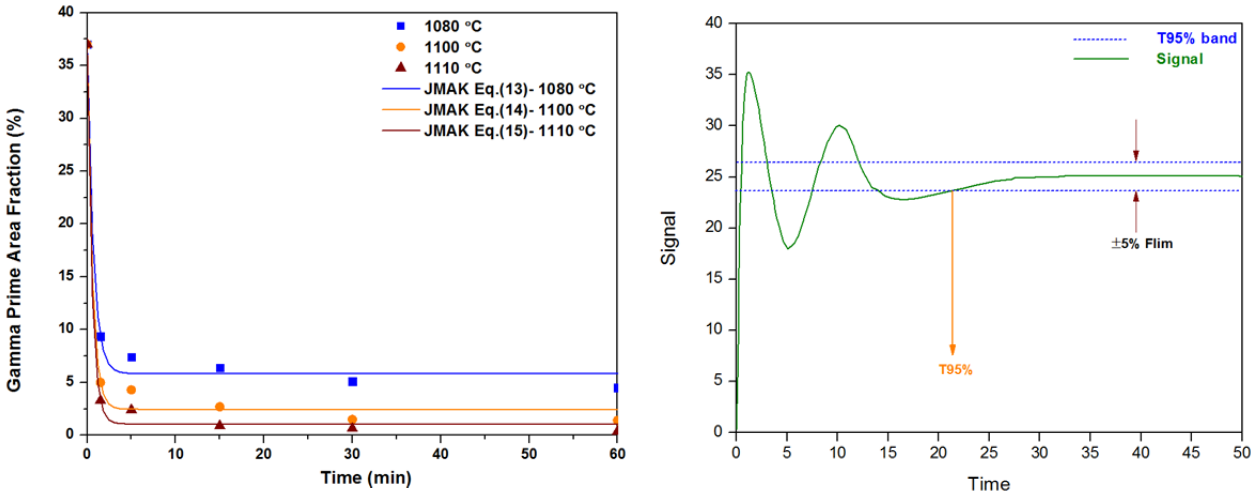

(a) (b)

Fig. 9. (a) Comparison of the multiple γ′ precipitate dissolution kinetics at 1080, 1100 and1110°C (b) Schematic of the T95%

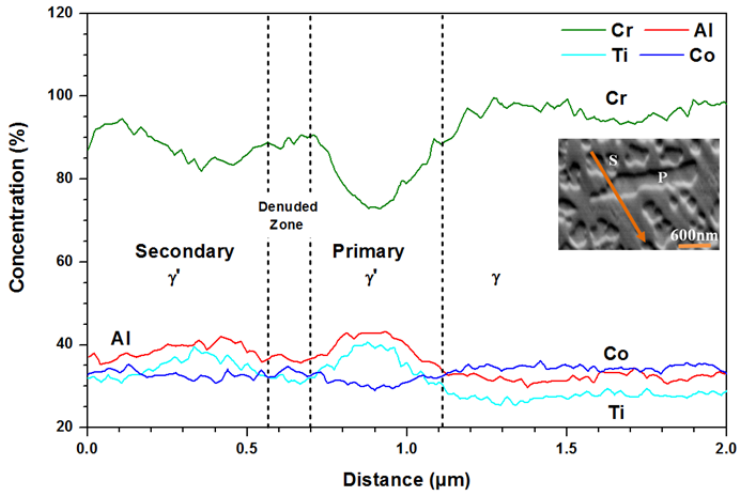

Fig. 10. Comparison of the Al, Ti, Co and Cr concentration profiles for large or primary (P) and small or secondary (S) γ′ particles using EDS line map analysis

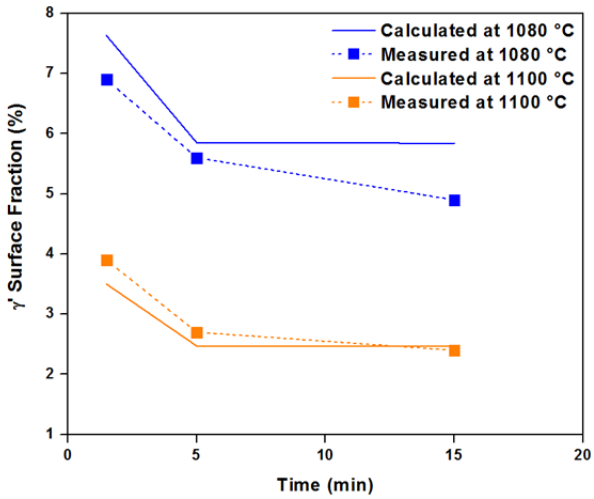

Fig. 11. Comparison of experimental data and theoretical prediction of γ′ surface fraction as a function of time at 1080 and 1100°C for low heating rate heat treatments

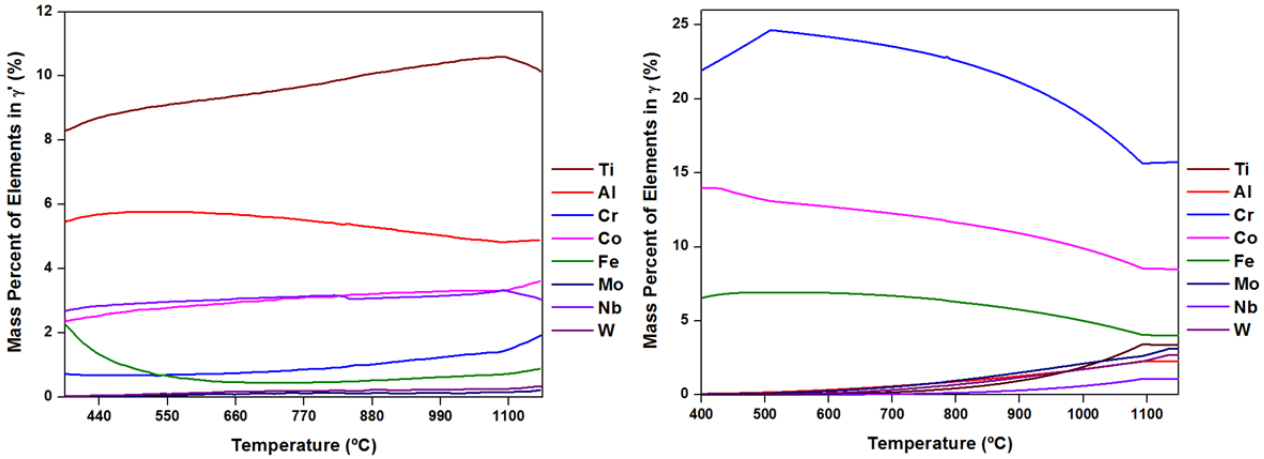

(a) (b)

Fig. 12. Calculated equilibrium composition of (a) γ′ phase (b) γ phase, as a function of temperature

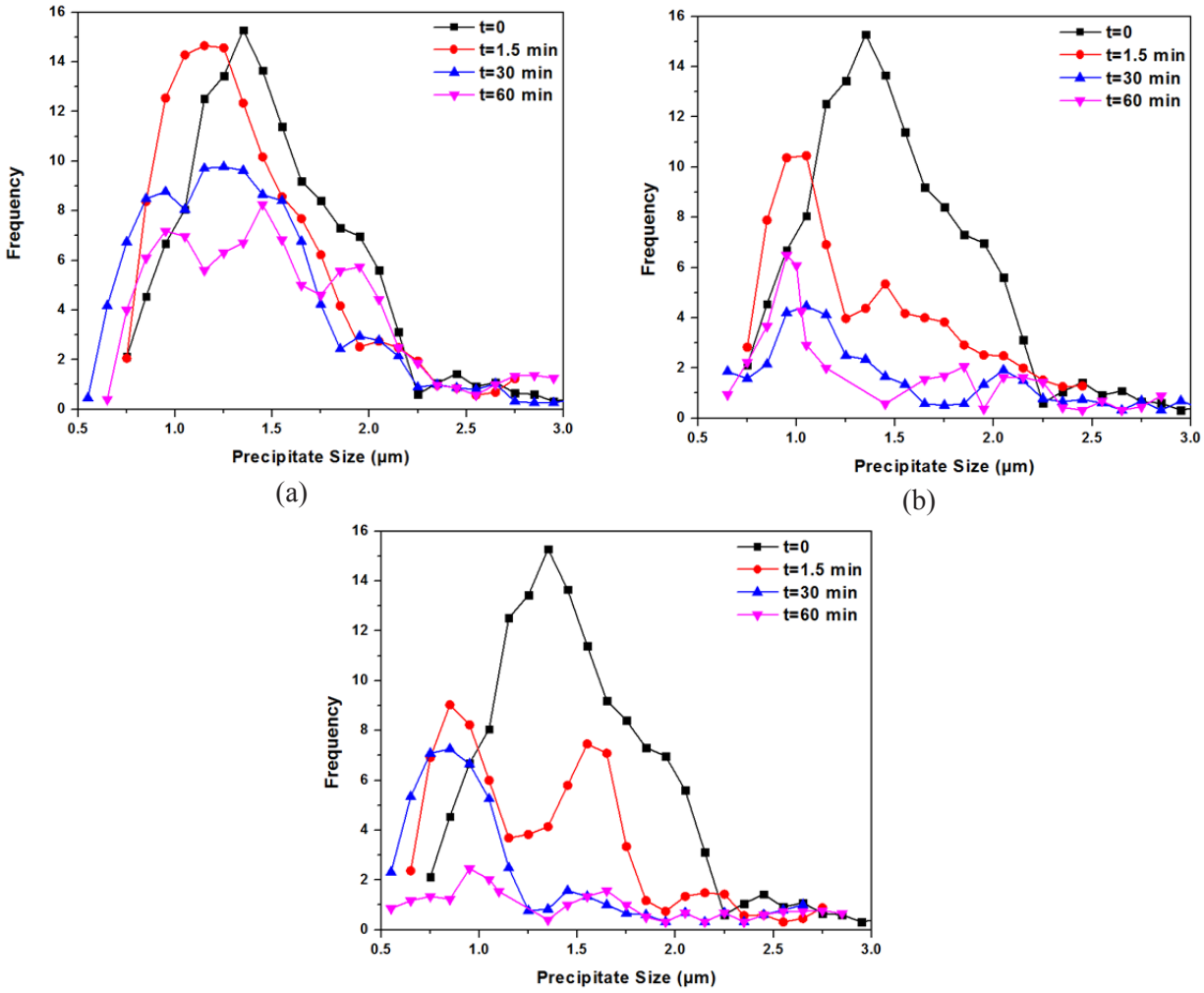

Fig. 13. Evolution of γ′ particle size distribution as a function of time at (a) 1080°C (b) 1100°C (c) 1110°C. The plot indicates that dissolution occurs for the first 1.5 minutes and coarsening takes place after 30 minutes holding time at 1080 and 1100°C. For heat treatment at 1110°C, only dissolution occurs at all holding times.

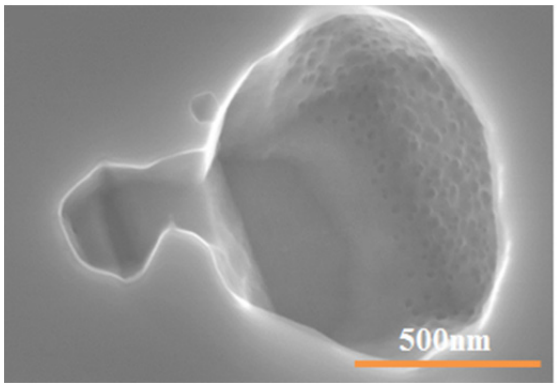

Fig. 14 Early stage of coalescence of two γ′ particles through diffuse neck at 1100°C for 5 minutes

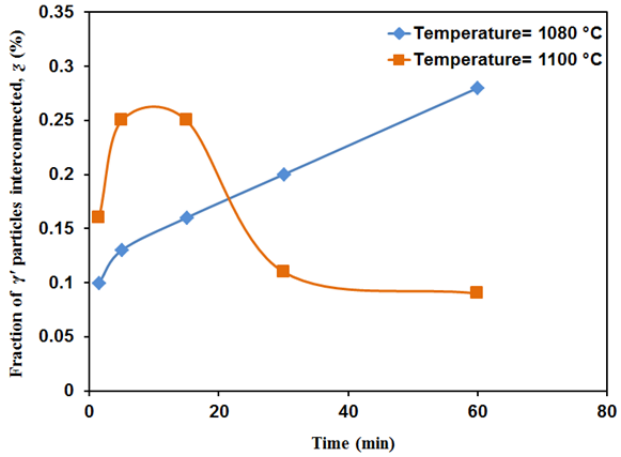

Fig. 15. The fraction of γ′ particles interconnected by neck as a function of holding time at 1080 and 1100°C

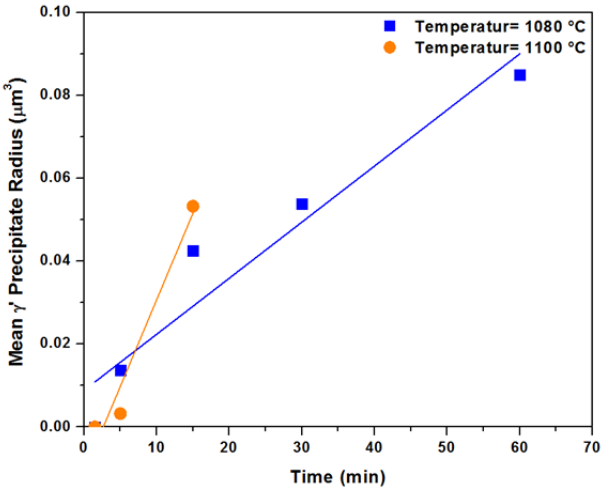

Fig. 16. Mean precipitate radius cubed, $\bar{r}^3$, as a function of holding time at 1080 and 1100°C. Points represent experimental values and the regression line shows there is a reasonable linear relationship (R^2 >0.93) between $\bar{r}^3$ and t.

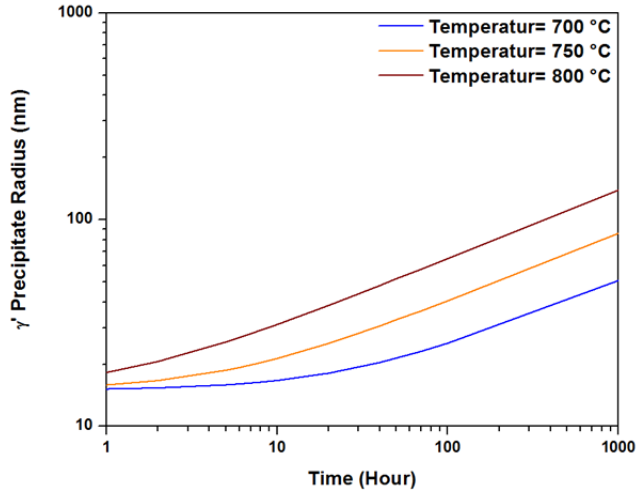

Fig. 17. Model predictions of γ′ precipitate radius as a function of aging time at 700, 750 and 800°C based on Eq.(24)

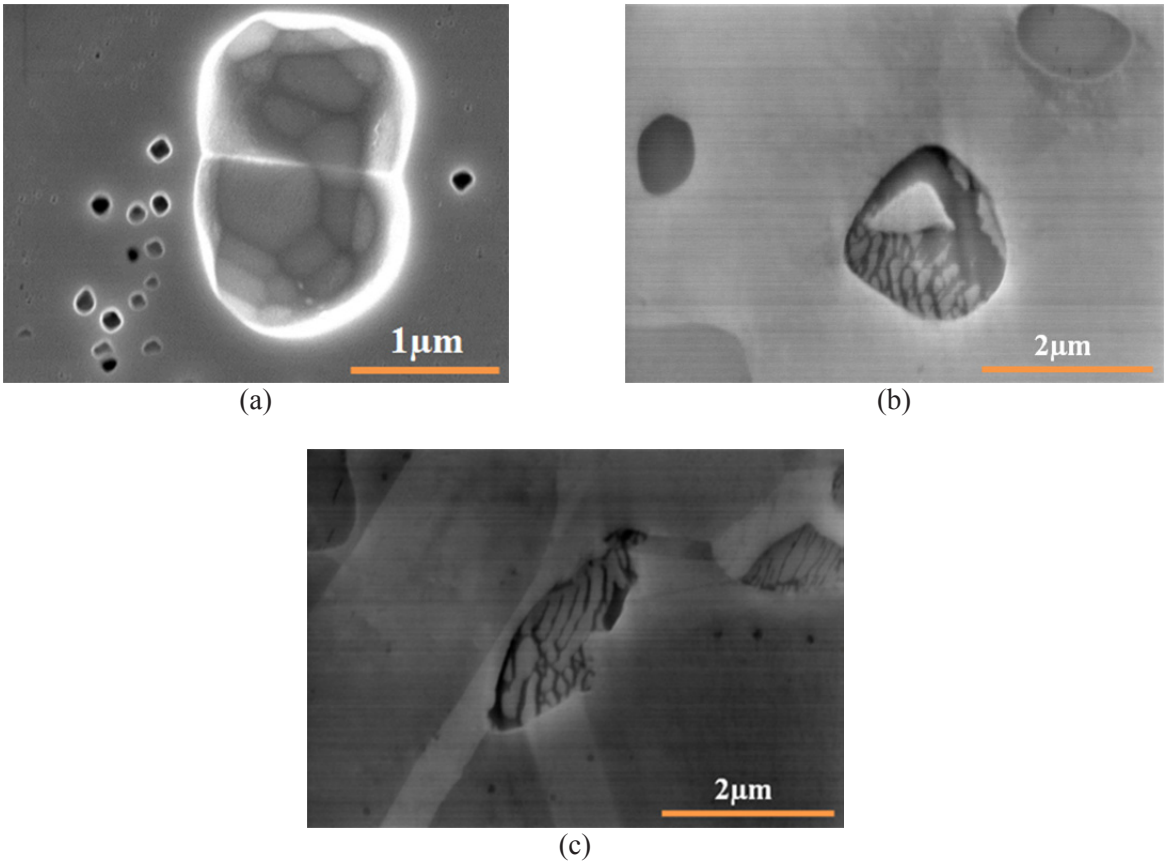

(a) (b)

(c)

Fig. 18. Various dissolution mechanisms a) Splitting (b) Dissolution from center and corner (c) Dissolution in the form of layers of γ and γ′

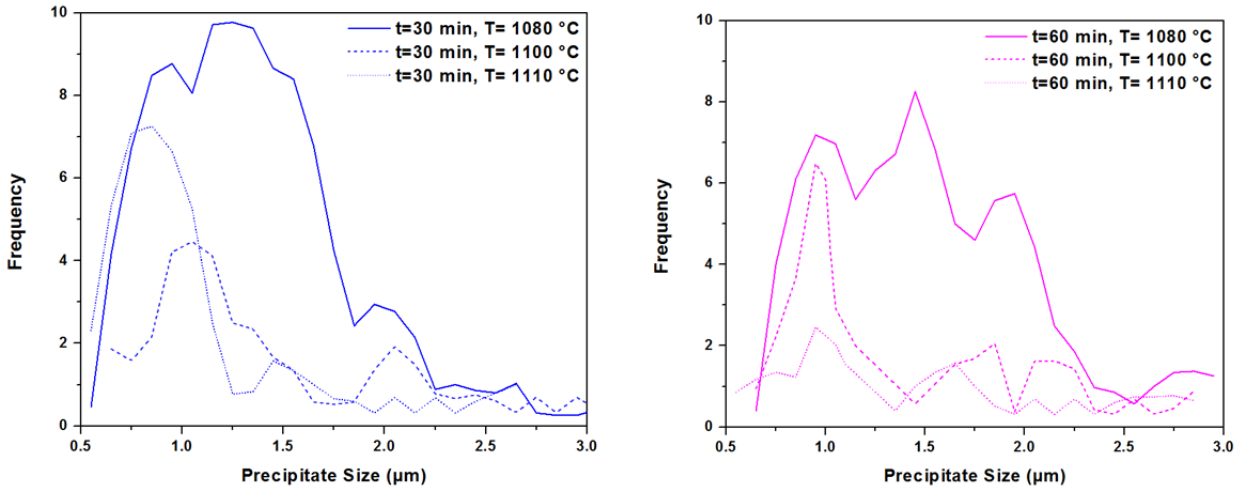

(a) (b)

Fig. 19. Comparison of γ′ particle size distribution at 1080, 1100 and 1110°C for (a) 30 minutes holding time (b) 60 minutes holding time. The plot indicates that breaking and splitting of larger particles into smaller ones occurs during heat treatment at 1110°C for 30 minutes holding time.